

Scattering of a short electromagnetic pulse from a Lorentz-Duffing film: theoretical and numerical analysis

Moysey Brio^{a,*}, Jean-Guy Caputo^b, Kyle Gwartz^c, Jinjie Liu^d, Andrei Maimistov^e

^a*Department of Mathematics, University of Arizona, Tucson, Arizona 85721*

^b*Laboratoire de Mathématiques, INSA Rouen Normandie, 76801 Saint-Etienne du Rouvray, France*

^c*Program in Applied Mathematics, University of Arizona, Tucson, Arizona 85721*

^d*Department of Mathematical Sciences, Delaware State University, Dover, DE 19901*

^e*Department of Solid State Physics and Nanostructures,
National Research Nuclear University, Moscow Engineering Physics Institute,
Kashirskoe sh. 31, Moscow, 115409 Russia*

Abstract

We combine scattering theory, Fourier, traveling wave and asymptotic analyses together with numerical simulations to present interesting and practically useful properties of femtosecond pulse interaction with thin films. The dispersive material is described by a single resonance Lorentz model and its nonlinear extension with a cubic Duffing-type nonlinearity. A key feature of the Lorentz dielectric function is that its real part becomes negative between its zero and its pole, generating a forbidden region. We illustrate numerically the linear interaction of the pulse with the film using both scattering theory and Fourier analysis. Outside this region we show the generation of a sequence of pulses separated by round trips in the Fabry-Perot cavity due to multiple reflections. When the pulse spectrum is inside the forbidden region, we observe total reflection. Near the pole of the dielectric function, we demonstrate the slowing down of the pulse (group velocity tending to zero) in the medium that behaves as a high-Q cavity. We use the combination of analysis and simulations in the linear regime to validate the delta function approximation of the thin layer; this collapses the forbidden region to a single resonant point of the spectrum. We also study the single cycle pulse interaction with a thin film and show three distinct types of reflection: half-pulse, sinusoidal wave train and cosine wavelet. Finally we analyze the influence of a strong nonlinearity and observe that the film switches from reflecting to transparent.

Keywords: Scattering theory, Lorentz-Duffing medium, Finite Difference Time Domain, femtosecond pulse

1. Introduction

The interaction of femtosecond pulses with thin dispersive nonlinear films has been a subject of numerous recent theoretical, numerical and experimental studies [1, 2, 25, 26, 27, 29]. For many transparent or weakly absorbent materials such as insulators, glasses, doped glasses, semiconductors and amorphous materials, the dielectric function can be often be described by a single resonance Lorentz model or a combination of such models [9, 10, 21, 22, 23]. Many such materials have negligible or zero damping coefficient (transparent Lorentz materials) [10]. One of the key features of the Lorentz dielectric function is that -between its zero and its pole- the real part is negative so that the wave vector is purely imaginary. This region of total reflection comes under different names, e.g. forbidden zone in quantum mechanics, non-propagating region in electromagnetic wave theory, stop band in optical filters, Restrahlen band in bulk solids with crystalline structure, and polaritonic gap in photonic crystals [5, 6, 7, 9]. This property is used in numerous applications: thin optical film filters, spectroscopic ellipsometry and artificial bulk and surface meta materials [11, 7, 8].

*Corresponding author

Email address: brio@math.arizona.edu (Moysey Brio)

In this article, we focus on the various consequences of the presence of the forbidden region on the interaction of a short pulse with the thin film. For the linear Lorentz oscillator model and an incident pulse, an exact analytic solution is available in integral form involving Green's functions, inverse Fourier and Laplace transforms. However it is difficult to extract useful design information from these complicated formulas; this requires either asymptotic analysis or various simplifying assumptions [12, 13]. In our study, we combine scattering theory, Fourier, traveling wave and asymptotic analyses together with one-dimensional finite-difference time-domain (FDTD) numerical simulations [3, 14, 15] to provide interesting and practically useful scattering properties of thin films. We illustrate numerically the linear interaction of the pulse with the film using both scattering theory and Fourier analysis. We show in particular, the generation of a sequence of pulses separated by round trips in the Fabry-Perot cavity due to multiple reflections, the total reflection and high-Q property of the cavity due to the slowing down (group velocity tending to zero) near the pole of the Lorentz dielectric function. The filtering property is shown for a pulse whose spectrum overlaps the forbidden zone. We continue this study by validating the delta function approximation of the thin layer. We also consider the interaction of a single cycle pulse with the thin film and show three possible types of reflection: half-pulse, sinusoidal wave train and cosine wavelet. Finally, a strong cubic Duffing-type polarization nonlinearity is studied. It demonstrates that the film switches from being totally reflecting to being transparent.

The article is organized as follows. Section 2 describes the Lorentz-Duffing model. Section 3 presents the FDTD algorithm to solve the one-dimensional Maxwell-Lorentz-Duffing equations and the numerical procedure to compute the scattering coefficients. In section 4, we review the scattering theory for the finite slab and the delta function approximation, compare the reflection coefficients for different slab thicknesses and describe the procedure to compute the scattering coefficients from the time series of the numerical solution. In section 5, we present numerical results for pulses with spectra near and within the forbidden region. We also consider a single cycle pulse interacting with the thin film and the switching effect of the strong nonlinearity. Conclusions are presented in the final section.

2. The model

We consider a simplified description of the interaction of an electromagnetic wave with a ferroelectric material. The Lagrangian density for the vector potential A and the polarization P is

$$L = \epsilon_0 \left(\frac{A_t^2}{2} - c^2 \frac{A_x^2}{2} \right) + \left[\frac{\tau^2}{\epsilon_0} \left(\frac{P_t^2}{2} - \alpha \frac{P^2}{2} - \beta \frac{P^4}{2} \right) - A_t P \right] \mathcal{I}(x), \quad (1)$$

where we have used dimensional quantities, where the subscripts indicate partial derivative, where τ is a characteristic time of the material, α and β are characteristic parameters of the ferroelectric and where $\mathcal{I}(x)$ is the indicator function of the material; for a slab $\mathcal{I}(x) = 1$, if $0 < x < w$, else $\mathcal{I}(x) = 0$. In [25], we had written a similar density but used dimensionless units.

The Euler-Lagrange equations are

$$\epsilon_0 (A_{tt} - c^2 A_{xx}) = P_t \mathcal{I}(x), \quad (2)$$

$$\frac{\tau^2}{\epsilon_0} (P_{tt} + \alpha P + \beta P^3) = -A_t, \quad (3)$$

where the second equation only exists in the medium. Introducing the electric field component $E = -A_t$ results in the dimensional system

$$\epsilon_0 (E_{tt} - c^2 E_{xx}) = -P_t \mathcal{I}(x), \quad (4)$$

$$\frac{\tau^2}{\epsilon_0} (P_{tt} + \alpha P + \beta P^3) = E, \quad (5)$$

We normalize E and P as $E = E_0 e$, $P = P_0 p$ and get our final system

$$e_{tt} - c^2 e_{xx} = -\frac{1}{\xi} p_{tt} \mathcal{I}(x), \quad (6)$$

$$p_{tt} + \alpha p + \beta P_0^2 p^3 = \frac{\xi}{\tau^2} e, \quad (7)$$

where we have introduced the dimensionless parameter

$$\xi = \frac{\epsilon_0 E_0}{P_0}. \quad (8)$$

The system of equations (6,7) describes the coupling of a wave to an oscillator. It appears in various applications, see Lamb's book [24] for examples in mechanics.

3. Finite difference time domain numerical procedure

The system (6,7) is solved using a standard Yee Finite Difference Time Domain (FDTD) algorithm [28] on a staggered space-time grid for the displacement field $D = \epsilon_0 E + P$ and the magnetic field H . The one-dimensional Maxwell-Lorentz-Duffing equations are

$$D_t = -H_x, \quad (9)$$

$$\mu H_t = -E_x, \quad (10)$$

$$D = \epsilon_0 E + P, \quad (11)$$

$$\frac{\tau^2}{\epsilon_0} (P_{tt} + \alpha P + \beta P^3) = E. \quad (12)$$

They are approximated using the following discretization to update in time H, P, D , and E fields, respectively,

$$\mu \frac{H_{j+\frac{1}{2}}^{n+\frac{1}{2}} - H_{j+\frac{1}{2}}^{n-\frac{1}{2}}}{\Delta t} = -\frac{E_{j+1}^n - E_j^n}{\Delta x}, \quad (13)$$

$$\frac{\tau^2}{\epsilon_0} \frac{P_j^{n+1} - 2P_j^n + P_j^{n-1}}{\Delta t^2} + \tilde{\alpha} P_j^n + \tilde{\beta} (P_j^n)^3 = E_j^n, \quad (14)$$

$$\frac{D_j^{n+1} - D_j^n}{\Delta t} = -\frac{H_{j+\frac{1}{2}}^{n+\frac{1}{2}} - H_{j-\frac{1}{2}}^{n+\frac{1}{2}}}{\Delta x}, \quad (15)$$

$$E_j^{n+1} = \frac{1}{\epsilon_0} (D_j^{n+1} - P_j^{n+1}), \quad (16)$$

$$\text{where } \tilde{\alpha} = \frac{\tau^2}{\epsilon_0} \alpha, \quad \tilde{\beta} = \frac{\tau^2}{\epsilon_0} \beta. \quad (17)$$

An array $H_{j+\frac{1}{2}}^{n+\frac{1}{2}}$ approximates an exact magnetic field evaluated at $x = (j + \frac{1}{2})\Delta x$ and $t = n\Delta t$. The other arrays for P, D , and E are interpreted similarly.

In the perfectly matched layer (PML) the E and H update equations are modified as follows [28],

$$\mu \frac{H_{j+\frac{1}{2}}^{n+\frac{1}{2}} - H_{j+\frac{1}{2}}^{n-\frac{1}{2}}}{\Delta t} = -\frac{E_{j+1}^n - E_j^n}{\Delta x} - \sigma_{j+\frac{1}{2}}^H \frac{H_{j+\frac{1}{2}}^{n+\frac{1}{2}} + H_{j+\frac{1}{2}}^{n-\frac{1}{2}}}{2}, \quad (18)$$

$$\epsilon \frac{E_j^{n+1} - E_j^n}{\Delta t} = -\frac{H_{j+\frac{1}{2}}^{n+\frac{1}{2}} - H_{j-\frac{1}{2}}^{n+\frac{1}{2}}}{\Delta x} - \sigma_j^E \frac{E_j^{n+1} + E_j^n}{2}, \quad (19)$$

with matched electric and magnetic conductivities, $\frac{\sigma^H(x)}{\mu} = \frac{\sigma^E(x)}{\epsilon} = \sigma(x)$, and cubic conductivity, $\sigma(x) = \left(\frac{x}{d}\right)^3$. The amplitude of the reflected wave drops gradually as the PML layer is widened. For example, with a 10 point wide PML layer the reflection amplitude is about $8 \cdot 10^{-5}$ and drops to $5 \cdot 10^{-6}$ for a PML layer with 100 points.

3.1. Stability

The linearized scheme above is conditionally stable for sufficiently small time-steps Δt . To quantify this, we performed a Von Neumann stability analysis of the linearized numerical method taking

$$\begin{bmatrix} E_j^n \\ H_j^n \\ P_j^n \\ D_j^n \end{bmatrix} = \begin{bmatrix} \hat{E} \\ \hat{H} \\ \hat{P} \\ \hat{D} \end{bmatrix} e^{i\omega n \Delta t - i k j \Delta x}. \quad (20)$$

The resulting dispersion relation is

$$\sin^2\left(\frac{1}{2}\omega\Delta t\right) + \frac{\mu c^2 \sin^2\left(\frac{1}{2}\omega\Delta t\right)}{\frac{\tau^2}{\epsilon_0} \left(-\frac{4 \sin^2\left(\frac{1}{2}\omega\Delta t\right)}{(\Delta t)^2}\right) + \tilde{\alpha}} = \left(c \frac{\Delta t}{\Delta x}\right)^2. \quad (21)$$

It can be seen as a modification of the free space dispersion relation

$$\sin^2\left(\frac{1}{2}\omega\Delta t\right) = \left(c \frac{\Delta t}{\Delta x}\right)^2. \quad (22)$$

The Courant-Friedrich-Levy (CFL) restriction in the free space, $c \frac{\Delta t}{\Delta x} \leq 1$, is replaced by the following time step restrictions under the requirement that $\sin^2\left(\frac{1}{2}\omega\Delta t\right) \leq 1$,

$$\Delta t^2 \leq \frac{\gamma - \sqrt{\gamma^2 - 16\tilde{\alpha}\mu\tau^2c^4(\Delta x)^2 \sin^2\left(\frac{1}{2}k\Delta x\right)}}{2\tilde{\alpha}c^2 \sin^2\left(\frac{1}{2}k\Delta x\right)}, \quad (23)$$

where

$$\gamma = (\tilde{\alpha} + c^2\mu)(\Delta x)^2 + 4c^4\mu\tau^2 \sin^2\left(\frac{1}{2}k\Delta x\right).$$

The figure below illustrates the dependence of the time step for fixed Δx as a function of the dispersion and nonlinearity parameters τ and α respectively. For sufficiently weak dispersive and nonlinear effects, the CFL restriction on the linear wave propagation, $\Delta t < \frac{\Delta x}{c^2}$ suffices, while for stronger dispersion and nonlinearities the time step has to be reduced to resolve these effects.

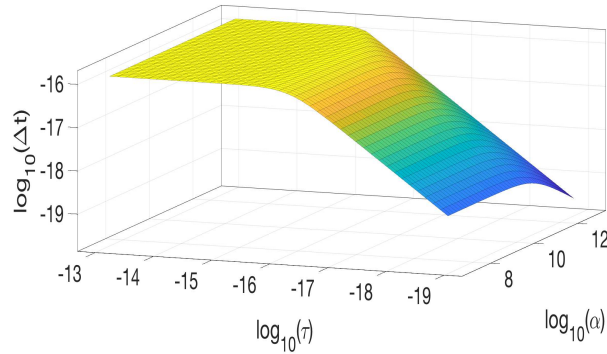


Figure 1: Stability surface of Δt as function of dispersion and nonlinearity parameters τ and α .

4. Scattering solution

In the linear regime the equations (6,7) reduce to

$$e_{tt} - c^2 e_{xx} = -\frac{1}{\xi} p_{tt} \mathcal{I}(x), \quad (24)$$

$$p_{tt} + \alpha p = \frac{\xi}{\tau^2} e, \quad (25)$$

where $\mathcal{I}(x)$ is the indicator function of the film. Then the solution can be computed using scattering theory using a plane wave Fourier decomposition of the solution, an approach standard for any linear dispersive system, see for example the scattering problem for the Schroedinger equation described in Dodd et al [30]. Writing e, p in harmonic form as

$$e(x, t) = e^{i\omega t} f(x), \quad p(t) = qe^{i\omega t}$$

we get the system

$$f_{xx} + k^2 f = -\frac{k^2}{\xi} \mathcal{I}q, \quad (26)$$

$$(\omega^2 - \alpha)q = -\frac{\xi}{\tau^2} f, \quad (27)$$

which can be reduced to

$$f_{xx} + f k^2 \left[1 + \frac{1}{\tau^2(\alpha - c^2 k^2)} \mathcal{I} \right] = 0. \quad (28)$$

In the slab $0 < x < L$, we have

$$f_{xx} + k_0^2 f = 0, \quad (29)$$

where

$$k_0 = k \sqrt{1 + \frac{1}{\tau^2(\alpha - c^2 k^2)}}. \quad (30)$$

To compute the reflection and transmission coefficients, one writes the solutions as a left field f^l , middle field f^m and right field f^r

$$f^l = e^{-ikx} + R e^{ikx}, \quad (31)$$

$$f^m = A \cos k_0 x + B \sin k_0 x, \quad (32)$$

$$f^r = T e^{-ikx}. \quad (33)$$

At the two interfaces, $x = 0, L$ the electric field and its derivative are continuous. To see this, integrate the operator on a small interval across the interface and take the limit of the interval going to zero. We then have the following interface conditions at $x = 0, L$

$$f^l(0) = f^m(0), \quad f^m(L) = f^r(L), \quad (34)$$

$$f_x^l(0) = f_x^m(0), \quad f_x^m(L) = f_x^r(L). \quad (35)$$

This gives four linear equations for the four unknowns R, T, A, B . Solving for R, T, A, B we get

$$R = \frac{(k^2 - k_0^2) \sin k_0 L}{D}, \quad T = \frac{2ik k_0 \exp ikL}{D}, \quad (36)$$

$$A = \frac{2k(-ik_0 \cos k_0 L + k \sin k_0 L)}{D}, \quad B = \frac{2k(k \cos k_0 L + ik_0 \sin k_0 L)}{D},$$

$$D = -2ik k_0 \cos k_0 L + (k^2 + k_0^2) \sin k_0 L. \quad (37)$$

4.1. Forbidden range and bound states

When examining the expressions (36) one sees that there are special values of k . One of them gives $k_0 = 0$ which corresponds to a pole of R and T , the corresponding solution is called a bound state. Another interesting k is such that $k_0 \rightarrow \infty$. These two values are shown in Fig. 2 where we plotted k_0 as a function of $\lambda = 2\pi/k$.

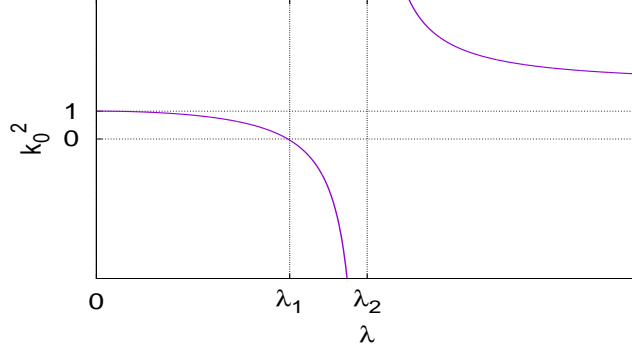


Figure 2: Plot of k_0^2 as a function of the wave-length λ .

We indicated the value λ_1 such that $k_0 = 0$ and the value λ_2 such that $k_0 \rightarrow \infty$. These are

$$\lambda_1 = 2\pi \frac{c\tau}{\sqrt{\alpha\tau^2 + 1}} = 2\pi \frac{c\tau}{\sqrt{\tilde{\alpha}\epsilon_0 + 1}}, \quad (38)$$

$$\lambda_2 = 2\pi \frac{c}{\sqrt{\alpha}} = 2\pi \frac{c\tau}{\sqrt{\tilde{\alpha}\epsilon_0}}, \quad (39)$$

$$(40)$$

In the region $[\lambda_1; \lambda_2]$, no propagation is possible inside the slab as the waves are exponentially damped because k_0 is purely imaginary.

Bound states correspond to imaginary $k = i\kappa$; then the field decays exponentially outside the slab. To find them, we substitute the following ansatz into the interface boundary conditions

$$f^l = e^{\kappa x}, \quad \kappa > 0 \quad (41)$$

$$f^m = A \cos \tilde{k}_0 x + B \sin \tilde{k}_0 x, \quad (42)$$

$$f^r = T e^{-\kappa x}. \quad (43)$$

The resulting solvability condition in terms of κ is as in [30],

$$\frac{-2\kappa\tilde{k}_0}{\kappa^2 - \tilde{k}_0^2} = \tan(\tilde{k}_0 L), \quad (44)$$

where

$$\tilde{k}_0 = \kappa \sqrt{1 + \frac{1}{\tau^2(\alpha + c^2\kappa^2)}}, \quad (45)$$

gives the nonlinear equation in terms of κ for bound states allowed. Note that the equation for \tilde{k}_0 is exactly as in (30) with $k = i\kappa$.

4.2. Thin slab : Dirac-delta function model

In the particular case where the film thickness L is small compared to λ , we approximate

$$\mathcal{I} \approx L\delta(x).$$

The system in harmonic component f (28) reduces to

$$f_{xx} + fk^2 \left[1 + \frac{1}{\tau^2(\alpha - c^2k^2)} L\delta(x) \right] = 0. \quad (46)$$

At $x = 0$, we assume continuity of f and have the jump condition for the first derivative of f as follows, from (24)

$$[f_x]_0^+ + \frac{k^2 f(0)L}{\tau^2(\alpha - c^2k^2)} = 0. \quad (47)$$

Using these two relations together with formulas for the solution on both sides of the slab, f^- , f^+ from (31), we recover the known reflection and transmission coefficients [25],

$$R = \frac{-kL}{G}, \quad T = \frac{2i\tau^2(\alpha - c^2k^2)}{G}, \quad (48)$$

$$G = 2i\tau^2(\alpha - c^2k^2) + kL \quad (49)$$

When $k^2 = \alpha/c^2$, we have resonance and full reflection, $T = 0$ and $R = -1$, while for values of k such that kL is small the reflection is negligible and $T \approx 1$.

To illustrate the range of validity of the delta function approximation of the finite slab, we computed the reflection coefficients of the delta function (48) and of the finite slab (36) for different thicknesses of the slab L . The results are plotted in Fig. 3.

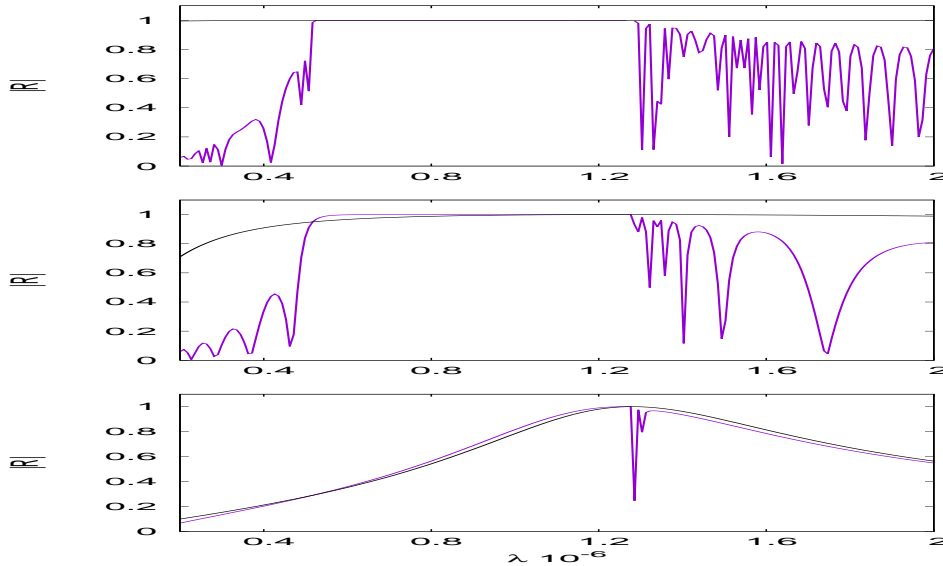


Figure 3: Modulus of reflection coefficient $|R(\lambda)|$ for a finite slab (blue online) and the delta function approximation (black) for widths $L = 5 \cdot 10^{-6}$ (top), $L = 5 \cdot 10^{-7}$ (middle) and $L = 5 \cdot 10^{-8}$ (bottom).

For $L = 5 \cdot 10^{-6}$, shown in the top panel of Fig. 3 the delta function approach gives a very poor approximation of the reflection coefficient. The middle panel of Fig. 3 shows the case $L = 5 \cdot 10^{-7}$. Again the

delta function approach fails to capture the fine features of the reflection coefficient. Only when $L = 5 \cdot 10^{-8}$, shown in the bottom panel of Fig. 3, do the exact and delta function approximation agree well. The delta function still fails to predict the dip due to the forbidden range.

One can estimate the scattering coefficients directly from the time-dependent problem (24). The numerical procedure for this is described in the next section.

4.3. Numerical computation of scattering data

We use the following algorithm to compute reflection and transmission coefficients R , and T .

1. Fix two observation points $x = a < 0$ and $x = b > L$ on each side of the layer.
2. Run the code and record the time history of the electric field at two observation points, $E(x = a, t)$, $E(x = b, t)$.
3. From the time-series $E(a, t)$ extract the incident pulse $E_i(t)$, stopping the recording before the arrival of the reflected pulse. Then obtain the remaining record at the observation point $x = a$ extract the time-series for the reflected pulse $E_r(a, t)$.
4. Take the Fourier transform (in practice the Fast Fourier Transform (FFT)) of $E_i(a, t)$, $E_r(a, t)$ and $E_t(b, t)$. These are denoted respectively as $\hat{E}_i(\omega)$, $\hat{E}_r(\omega)$, $\hat{E}_t(\omega)$.

The reflection and transmission coefficients are

$$R(\omega) = \frac{\hat{E}_r(\omega)}{\hat{E}_i(\omega)}, \quad T(\omega)e^{i\omega(b-a)} = \frac{\hat{E}_t(\omega)}{\hat{E}_i(\omega)}, \quad (50)$$

where the phase correction factor arises because the incident pulse is recorded at location $x = a$, while the transmitted pulse is observed at $x = b$.

5. Numerical results

In most of our numerical experiments, the spatial domain is $[0; \mathcal{L}]$, with $\mathcal{L} = 10^{-4}$. The discretization was done with 2500 uniform intervals except for the single cycle pulse case described later. The time step $\Delta t = \Delta x / (4c)$ satisfies the stability conditions. We chose the parameters shown in table 1 unless stated otherwise, as in the case of strong nonlinearity.

α (s^{-2})	L (m)	τ (s)	σ	λ (m)
$1.95 \cdot 10^{31}$	$5 \cdot 10^{-6}$	$3 \cdot 10^{-16}$	$14 \cdot 10^{-15}$	$0.4 \cdot 10^{-6} \leq 1.6 \cdot 10^{-6}$

Table 1: *Physical parameters.*

For these parameters, the critical wavelengths corresponding to the forbidden region $[\lambda_1, \lambda_2]$ are

$$\lambda_1 = 0.517 \cdot 10^{-6}, \quad \lambda_2 = 1.280 \cdot 10^{-6}. \quad (51)$$

The initial pulse propagates from the left to the right and is produced by the source of the following form, placed two grid points away from the PML layer

$$E(t) = e^{-(t/\sigma)^2} \sin(\omega t). \quad (52)$$

We begin our numerical examples by illustrating the pulse behavior when its spectrum is slightly below, within, and slightly above the forbidden region for three values of center wavelength λ near the gap.

5.1. Reflection and transmission : $\lambda = 0.410^{-6} < \lambda_1$

We first examine a pulse whose spectrum of below the forbidden region, see Fig. 5.

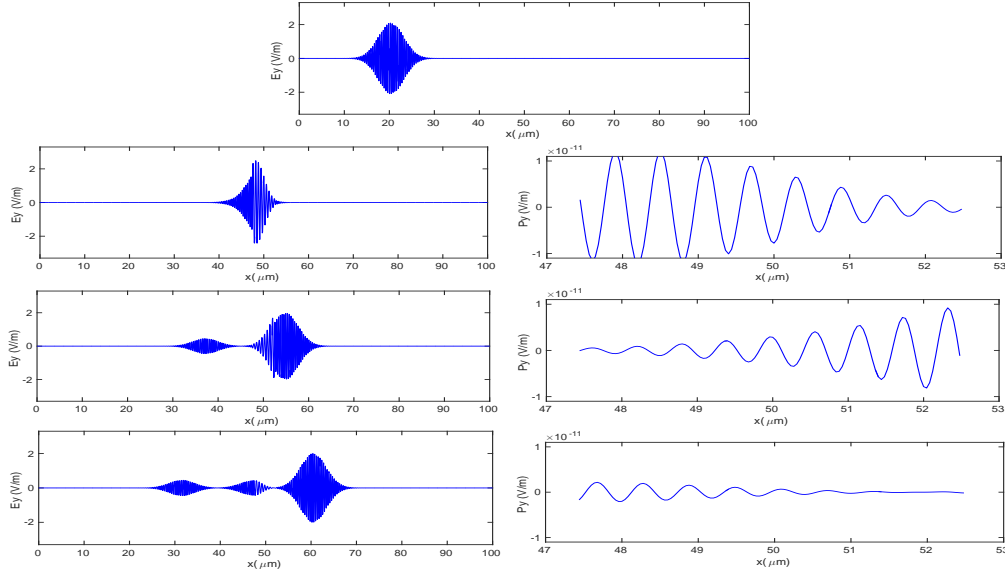


Figure 4: Reflection / transmission of a pulse : snapshots of the solution $E(x,t)$ and $P(x,t)$ inside the slab for $t = 10^{-13}$, $2 \cdot 10^{-13}$, $2.3 \cdot 10^{-13}$ and $2.5 \cdot 10^{-13}$ (top to bottom).

Fig. shows snapshots of the electric field $E(x,t)$ (left column) and polarization $P(x,t)$ (right column). The medium is located in the region $[47.5; 52.5] \mu\text{m}$. The first row shows the initial pulse. In the second row, as the pulse penetrates the slab, we see partial reflection. The polarization is sloshing between the left and the right boundaries of the medium generating a sequence of reflected pulses as shown in the subsequent rows. This dynamics is in accordance with the single frequency reflection/transmission theory for the Fabry-Perot cavity [32].

The reflection coefficient is shown in Fig. 5.

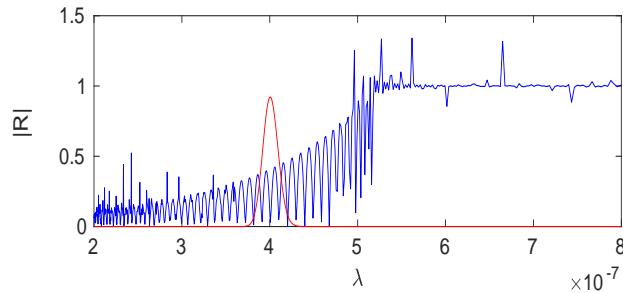


Figure 5: Reflection coefficient $|R(\lambda)|$ together with $20 \times |\hat{E}_i|$. Same parameters as Fig. 5.1.

Notice that even though the spectrum of the initial pulse is band limited, we recover the full theoretical spectrum $[\pi/\Delta x, -\pi/\Delta x]$. This is because of the numerical noise induced by the round-off errors and the discontinuity in the initial pulse on the order of the time step Δt .

5.2. Total reflection in the forbidden range : $\lambda_1 < \lambda = 0.610^{-6} < \lambda_2$

For this value of the centered wavelength λ , the pulse spectrum is in the region of total reflection 6 and the pulse is completely reflected as shown in Fig. 6. The polarization decays exponentially inside the medium.

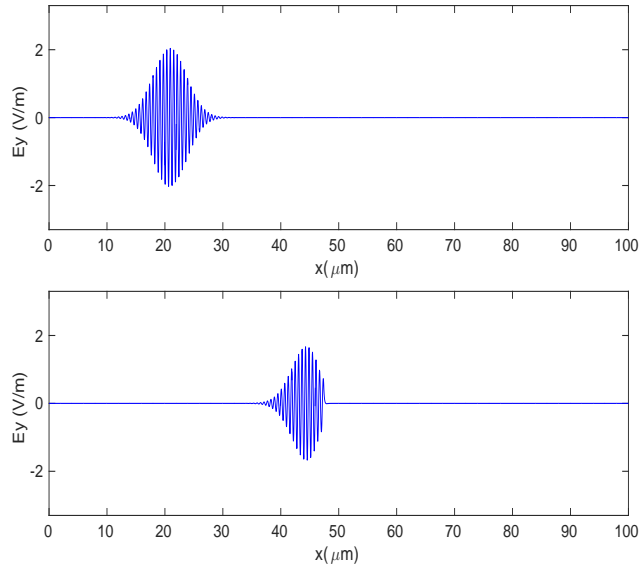


Figure 6: Total reflection of a pulse : snapshots of the solution $E(x, t)$ for $t = 10^{-13}$ and $t = 2 \cdot 10^{-13}$ (top to bottom).

As expected, the reflection coefficient is equal to 1 as seen in Fig. 7.

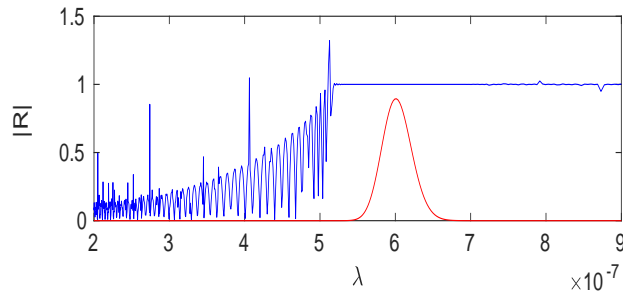


Figure 7: Reflection coefficient $|R(\lambda)|$ together with $20 \times |\hat{E}_i|$. Same parameters as Fig. 6.

Notice again that we capture the full theoretical spectrum.

5.3. Scattering close to bound state $\lambda_2 < \lambda = 1.410^{-6}$

For the values of λ near the pole λ_2 , the group velocity $c\sqrt{(\alpha - \tau^2 c^2 k^2)}/\alpha$ is near zero so that the wave is considerably slowed down inside the slab which behaves as a high-Q cavity radiating long harmonic wave trains. In Fig. 8, the initial pulse is shown in the first row. The snapshots in time are shown in the subsequent rows for the electric field (left column) and the polarization inside the slab (right column). In the second row, the reflected pulse is leaving the computational domain and the wave inside the slab has not

yet reached the right boundary of the slab. The film acts as a low-pass filter due to the overlap of the pulse spectrum with the forbidden zone. Fig. 9 shows the theoretical reflection coefficient, exhibiting a singularity for $\lambda = \lambda_2$ and zeroes at k such that $\sin k_0 L = 0$. As can be seen, the zeroes of $|R|$ accumulate near the pole λ_2 .

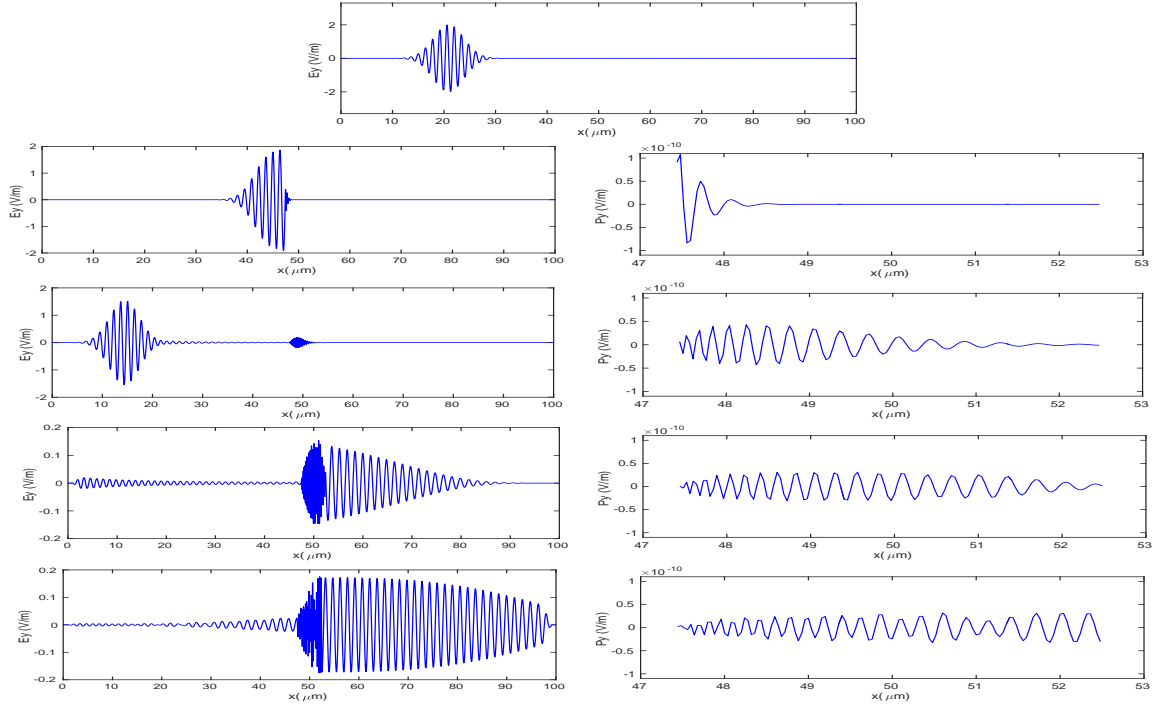


Figure 8: Reflection / transmission of a pulse : snapshots of the solution $E(x,t)$ and $P(x,t)$ inside the slab for $t = 10^{-13}, 2 \cdot 10^{-13}, 3 \cdot 10^{-13}, 4 \cdot 10^{-13}$ and $5 \cdot 10^{-13}$ (top to bottom).

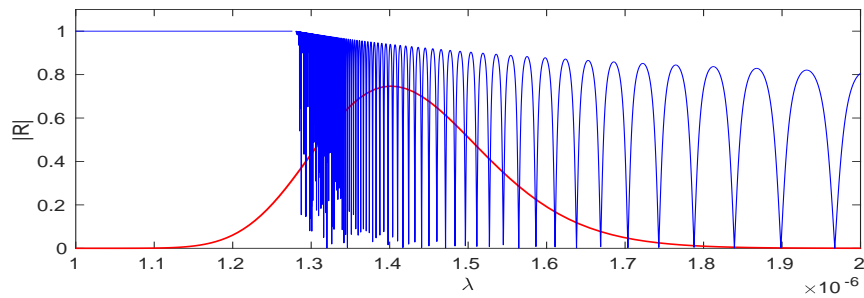


Figure 9: Theoretical reflection coefficient $|R(\lambda)|$ from (36) together with $20 \times |\hat{E}_i|$. The parameters are the same as in Fig. 8.

5.4. Reflection of a single cycle incident pulse

In [29] it was shown that a one cycle incident pulse may generate a half-pulse reflected wave for a very thin film. In this section we generalize this result by demonstrating three distinct reflection regimes arising

when a single cycle pulse impinges on a thin Lorentz dispersive layer. To see this, we consider the full Maxwell-Lorentz equations. The exact solution of the one-dimensional wave equation with a source P_{tt} is equal to the double integral of the source in space and time, 4 and assuming additionally a delta function in space leaves only time integration [29]. This implies that the reflected wave is proportional to P_t [29]. Consider the polarization equation 5 with a source equal to the single cycle incident pulse (52). There are three distinct regimes.

1. If P_{tt} is the dominant term, then $P_{tt} \approx E$ so that P_t is equal to the integral of the incident pulse, resulting in a half-pulse reflection.
2. When the terms P_{tt} and P are of comparable size, the layer behaves as a harmonic source in time and generates a sinusoidal wave train.
3. Finally, when P is the dominant term in the polarization equation, then $P \approx E$ so that P_t is the time derivative of the incident pulse and is similar to the second derivative of a Gaussian pulse, also called a cosine wavelet.

We solved the interaction of a single cycle incident pulse with a thin Lorentz media layer numerically for a slab of thickness $L = 2 \cdot 10^{-8}$ and chose a resolution of 20 uniformly distributed points across the slab. Fig. 10 illustrates the three distinct possibilities for the reflected wave. The left column of Fig. 10 contains both the transmitted and reflected waves, while the right column shows the blow-ups of the reflected waves. Row 2 shows a half-pulse reflected wave of amplitude of about 20% of the original pulse, this is case 1. Row 3 shows a sinusoidal wave train generated by the oscillating polarization in the film as in case 2. Finally, row 3 shows the cosine wavelet that has amplitude of about 0.01% of the original pulse, as in case 3. It cannot be seen on the plot together with the transmitted wave due to the disparity of the amplitude scales.

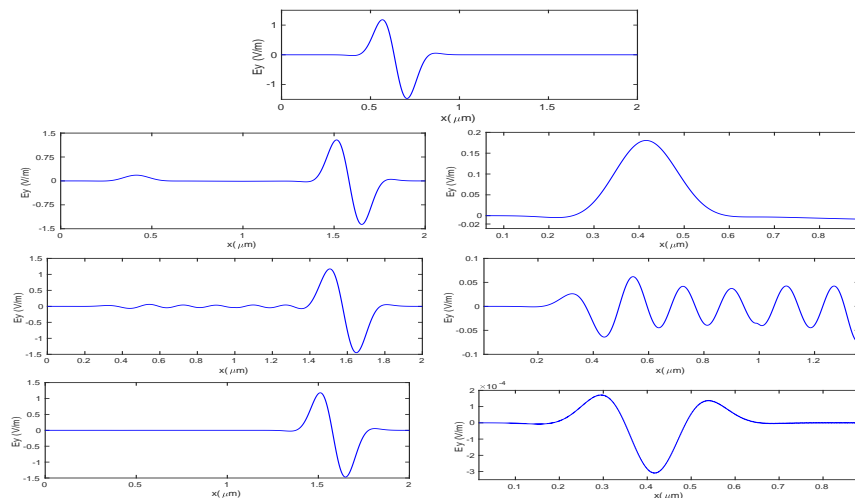


Figure 10: *Single cycle pulse interaction with a thin film. Initial pulse (top), transmitted and reflected pulses and blow-up of the reflected wave for $\tilde{\alpha} = 1.156 \cdot 10^9$ (2nd row), $\tilde{\alpha} = 1.156 \cdot 10^{12}$ (3rd row) and $\tilde{\alpha} = 1.156 \cdot 10^{14}$ (4th row). The width of the initial pulse is $\sigma = 0.43 \cdot 10^{-15}$ and the width of the layer is $L = 2 \cdot 10^{-8}$. The other parameters are the same as in table 1.*

5.5. Nonlinear effects

In this subsection, we show that a strong cubic nonlinearity of the Duffing form P^3 added to the linear Lorentz model may switch the thin film from being metal-like and totally reflective to becoming completely transparent. We start with a numerical illustration and proceed with an analytic explanation of this phenomenon. Consider a strongly nonlinear medium described by the coefficient $\beta = 10^{40}$ so that the terms

αP and βP^3 are of the same order. We choose a pulse center wavelength $\lambda = 9 \cdot 10^{-7}$ such that the pulse spectrum is in the forbidden band (the pulse width is as in Table 1).

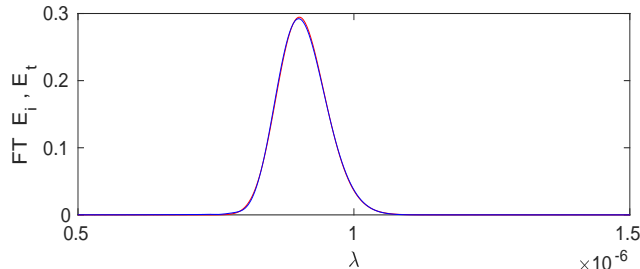


Figure 11: Modulus of the Fourier transform of the incoming pulse and the transmitted pulse as a function of λ .

When $\beta = 0$, the pulse gets reflected by the slab as described by the linear theory reviewed above. On the other hand, when $\beta = 10^{40}$ the pulse goes right through the slab with no visible reflection. Fig. 11 shows the Fourier transforms of both the incoming and transmitted fields. They are nearly indistinguishable on the plotted scale.

The heuristic explanation of this phenomena is that in the linear regime, reflection occurs due to destructive interference between the polarization and the field, whereas strong nonlinearity will change the frequency of the polarization and prevent this interference. The medium then becomes transparent. To justify this more rigorously, consider traveling waves for both the electric field and the polarization. Let $E(x-st)$ and $P(s-st)$ and set $\epsilon = 1/\beta \ll 1$ as a small parameter. Then the polarization equation becomes

$$(-s^2 + \alpha)\epsilon P + P^3 = \epsilon E.$$

Expanding in ϵ we obtain

$$P = (\epsilon E)^{1/3} + O(\epsilon^{2/3}).$$

For the traveling wave solutions, the wave equation reduces to

$$-s^2 E + E_{xx} = -s^2 P.$$

After substituting P , it becomes in the leading order $O(1)$

$$-s^2 E + E_{xx} = 0$$

which is exactly the wave equation in the traveling frame outside the film. Therefore to leading order in ϵ the incident pulse is not influenced by the thin film.

6. Conclusion

We have applied theoretical analysis and numerical simulations to present interesting and practically useful scattering properties of femtosecond pulses interacting with linear and nonlinear thin films. Combining scattering theory with numerical Fourier analysis we obtain a consistent picture of the filtering, multiple reflection, total reflection and high-Q cavity regimes observed for a finite width linear film. We also examined the validity of the delta function approximation and described three possible reflection scenarios for a single cycle pulse impinging on the thin film. Finally we presented a nonlinear switching effect.

Several observations came as a result of our study. The delta function approximation of the medium is accurate if the central wavelength of the pulse is about an order of magnitude larger than the width of the layer; this approximation shrinks the forbidden region to a single resonant wavelength. The generation of

a half-pulse from a single cycle incident pulse is sensitive to the parameters of the medium. Three distinct reflections are possible, the half-pulse, the sinusoidal wave train and the cosine wavelet. In the absence of a dominant term in the polarization equation, a combination of these three types of solutions will be present. A strong nonlinearity effectively changes the refractive index of the film making it very close to the refractive index of the outside medium. This results in a nearly perfectly transparent nonlinear film.

7. Acknowledgments

M. B. thanks INSA de Rouen for an invited professorship in the spring of 2018. The work of M.B. and J.L. were supported in part by the Air Force Office of Scientific Research under award number and FA9550-16-1-0199. J.-G. C. was supported by the Fractal Grid project from Agence Nationale de la Recherche.

References

- [1] I. V. Belousov, P. I. Khadzhi, A. V. Corovai and D. A. Markov, "Nonlinear transmission and reflection of ultrashort laser pulses by a thin semiconductor film under two-photon generation of bi-excitons", *Journal of Physics: Condensed Matter*, **23**, 22, 225802, (2011).
- [2] P. U. Jepsen, D. G. Cooke, and M. Koch, Terahertz spectroscopy and imaging Modern techniques and applications, *Laser Photonics Reviews*, 5 pp. 124166, 2011.
- [3] D.I. Blokhinchev, *Foundation of Quantum Mechanics*, Nauka, Moscow, 1976, chapter 9 .
- [4] T. W. H. Oates*, L. Ryves, and M. M. M. Bilek, Dielectric functions of a growing silver film determined using dynamic in situ spectroscopic ellipsometry, *Optics Express*, 16, p.2302 , 2008.
- [5] H. A. Macleod, *Thin-Film Optical Filters*, CRC Press, 4th ed. 2010.
- [6] J. Patterson and B.C. Bailey, *Solid-State Physics: Introduction to the Theory*, Springer, 2010.
- [7] A. Rung, Destruction of a polaritonic gap in a 2D photonic crystal, *Optics Communications* 252 , pp. 329-335, (2005).
- [8] B. Askenazi, A. Vasanelli, A. Delteil, Y. Todorov, L. C. Andreani, G. Beaudoin, I. Sagnes and C. Sirtori, Ultra-strong light-matter coupling for designer Reststrahlen band, *New J. Physics*, 16, pp. (2014).
- [9] M. Fox, *Optical Properties of Solids*, Oxford Univ. Press, 2nd ed., 2010.
- [10] http://www.horiba.com/fileadmin/uploads/Scientific/Downloads/OpticalSchool_CN/TN/ellipsometer/Lorentz_Dispersion_Model.pdf
- [11] H.G. Harland and E.A. Irene, *Handbook of Ellipsometry*, Springer, 2005
- [12] B. Gralak, M. Lequime, M. Zerrad, and C. Amra, Phase retrieval of reflection and transmission coefficients from kramer-skronig relations, *J. Opt. Soc. Am. A* 32, 456 (2015).
- [13] E. Bleszynski, M. Bleszynski and T. Jaroszewicz, Fast Time-Domain Integral Equation Approach for Wide-Band Pulse Propagation in Dispersive Media, *Ultra-Wideband Short-Pulse Electromagnetics*, 6, pp. 143-158, 2003
- [14] V. N. Vasil'ev, S. A. Kozlov, P. A. Petroshenko, and N. N. Rozanov, Self-Broadening of Space-Time Spectra of Few-Cycle Pulses in Dielectric Media. *Optics and Spectroscopy* **96**, 182-186 (2004).
- [15] A. A. Drozdov, S. A. Kozlov, A. A. Sukhorukov, and Yu.S. Kivshar. Self-phase modulation and frequency generation with few-cycle optical pulses in nonlinear dispersive media. *Phys.Rev. A* **86**, 053822 (2012).
- [16] N. N. Rozanov, Propagation of Short Pulses in a Medium with Frequency Dispersion, *Optics and Spectroscopy*, **92**, 239-242 (2002).
- [17] H. Leblond, D. Mihalache, Models of few optical cycle solitons beyond the slowly varying envelope approximation. *Physics Reports* **523**, 61;96;126 (2013).
- [18] J C Eilbeck, Reflection of short pulses in linear optics *J.Phys. A*5, 1355 - 1363 (1972).
- [19] Rupasov, V.I., and Yudson, V.I.: On the boundary problems of nonlinear optics of resonant media, *Kvant. Elektron.* **9**, 2179–2186 (1982) [*Sov. J. Quantum Electron.* **12**, 415–419 (1982)].
- [20] Benedict, M.G., Malyshev, V.A., Trifonov, E.D., and Zaitsev, A.I.: Reflection and transmission of ultrashort light pulses through a thin resonant medium: local-field effects, *Phys. Rev.* **A43**, 3845–3853 (1991).
- [21] N. N. Rozanov, Reflection of Ultrashort Pulses from the Boundary of a Drude-Lorentz Medium, *Optics and Spectroscopy* **94**, 396-399 (2003)
- [22] M. P. Sorensen, G. M. Webb, M. Brio and J. V. Moloney, Kink shape solutions of the Maxwell-Lorentz system. *Phys.Rev. E* **71**, 036602 (5 pages) (2005).
- [23] V. A. Trofimov, I.V. Mishanov, Reflection and propagation of laser pulse with a few cycles in medium with time-dependent dielectric permittivity, *Proc. SPIE* **8772**, *Nonlinear Optics and Applications VII*, 877211 (8 May 2013); doi: 10.1117/12.2017180
- [24] G. L. Lamb, "Elements of soliton theory", J. Wiley, (1980).
- [25] J.-G. Caputo, E. V. Kazantseva, A.I. Maimistov, "Electromagnetically induced switching of ferroelectric thin films", *Phys. Rev. B* 75, 014113, (2007).
- [26] J.-G. Caputo, A.I. Maimistov, E.D. Mishina, E.V. Kazantseva, V.M. Mukhortov, "High frequency polarization switching of a thin ferroelectric film", *Phys. Rev. B* 82, 094113, (2010).
- [27] E. V. Kazantseva and A. I. Maimistov, On the Passage of an Extremely Short Electromagnetic Pulse through a Ferroelectric Layer Embedded in a Paraelectric. *Optics and Spectroscopy*, 113, 550;96;555 (2012).

- [28] A. Taflove and S. C. Hagness, "Computational electrodynamics: the finite difference time domain method", (3rd edition), Artech House, (2005).
- [29] M. V. Arkhipov, R. M. Arkhipov, A. V. Pakhomov, I. V. Babushkin, A. Demircan, U. Morgner and N. N. Rosanov, "Generation of unipolar half-cycle pulses via unusual reflection of a single cycle pulse from an optically thin metallic or dielectric layer", *Optics Letters* **42**, 2189-2192, (2017).
- [30] R. Dodd, J. C. Eilbeck, J. D. Gibbon and H. C. Morris, "Solitons and nonlinear wave equations", Academic press, (1982).
- [31] W. Ames, "Numerical Methods for Partial Differential Equations", Academic Press, (1992).
- [32] J. M. Vaughan, "The Fabry-Perot Interferometer: History, Theory, Practice and Applications", Taylor & Francis, (1989).

